Structural basis for understanding oncogenic p53 mutations and designing rescue drugs

Andreas C. Joerger, Hwee Ching Ang, and Alan R. Fersht*

Cambridge University Chemical Laboratory and Cambridge Centre for Protein Engineering, Medical Research Council Centre, Hills Road, Cambridge CB2 2QH, United Kingdom

Contributed by Alan R. Fersht, August 22, 2006

The DNA-binding domain of the tumor suppressor p53 is inactivated by mutation in ≈50% of human cancers. We have solved high-resolution crystal structures of several oncogenic mutants to investigate the structural basis of inactivation and provide information for designing drugs that may rescue inactivated mutants. We found a variety of structural consequences upon mutation: (*i*) the removal of an essential contact with DNA, (*ii*) creation of large, water-accessible crevices or hydrophobic internal cavities with no other structural changes but with a large loss of thermodynamic stability, (*iii*) distortion of the DNA-binding surface, and (*iv*) alterations to surfaces not directly involved in DNA binding but involved in domain–domain interactions on binding as a tetramer. These findings explain differences in functional properties and associated phenotypes (e.g., temperature sensitivity). Some mutants have the potential of being rescued by a generic stabilizing drug. In addition, a mutation-induced crevice is a potential target site for a mutant-selective stabilizing drug.

cancer | crystal | structure | drug design | polymorphism

The tumor suppressor protein p53 is a 393-aa transcription factor that regulates the cell cycle and plays a key role in the prevention of cancer development. In response to oncogenic and other stresses, p53 induces the transcription of a number of target genes, resulting in cell-cycle arrest, senescence, or apoptosis (1, 2). In ≈50% of human cancers, p53 is inactivated as a result of missense mutation in the p53 gene (3, 4).

The multifunctionality of p53 is reflected in the complexity of its structure. Each chain in the p53 tetramer is composed of several domains. There are well defined DNA-binding and tetramerization domains and highly mobile, largely unstructured regions (5–9). Most p53 cancer mutations are located in the DNA-binding core domain of the protein (3). This domain has been structurally characterized in complex with its cognate DNA by x-ray crystallography (5, 10, 11) and in its free form in solution by NMR (12). It consists of a central β-sandwich that serves as a basic scaffold for the DNA-binding surface. The DNA-binding surface is composed of two large loops (L2 and L3) that are stabilized by a zinc ion and a loop–sheet–helix motif. Together, these structural elements form an extended surface that makes specific contacts with the various p53 response elements. The six amino acid residues that are most frequently mutated in human cancer are located in or close to the DNA-binding surface (compare release R10 of the TP53 mutation database at www-p53.iarc.fr) (3). These residues have been classified as "contact" (Arg-248 and Arg-273) or "structural" (Arg-175, Gly-245, Arg-249, and Arg-282) residues, depending on whether they directly contact DNA or play a role in maintaining the structural integrity of the DNA-binding surface (Fig. 1) (5).

Urea denaturation studies have shown that the contact mutation R273H has no effect on the thermodynamic stability of the core domain, whereas structural mutations substantially destabilize the protein to varying degrees, ranging from 1 kcal/mol for G245S and 2 kcal/mol for R249S up to >3 kcal/mol for R282W (13). The destabilization has severe implications for the folding state of these mutants in the cell. Because the wild-type core domain is only marginally stable and has a melting temperature only slightly above body temperature, highly destabilized mutants such as R282W are largely unfolded under physiological conditions and, hence, are no longer functional (14).

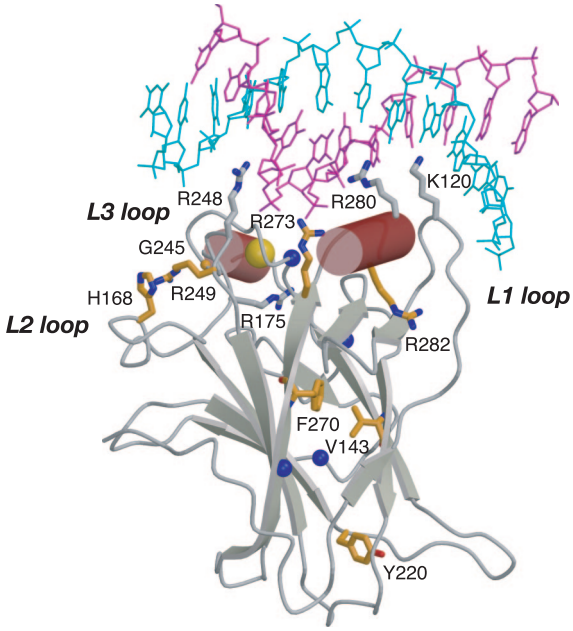

Fig. 1. Structure of the p53 core domain bound to consensus DNA (5). The two strands of bound consensus DNA are shown in blue and magenta. The bound zinc ion is displayed as a golden sphere. Cancer mutation sites that were structurally studied in this work and earlier work (16) are shown in orange. The blue spheres indicate the location of the mutation sites in the superstable quadruple mutant M133L/V203A/N239Y/N268D (*T*-p53C).

To understand the role of individual mutants in carcinogenesis and to assess the possibility of rescuing their function, it is important to know the effect of the mutation not only on the overall stability but also on the local structure. Qualitative NMR studies indicate that hotspot mutants evince characteristic local structural changes (15). We have recently elucidated the structural effects of the contact mutation R273H and the structural mutation R249S by x-ray crystallography (16). In addition, these structural studies revealed that the second-site suppressor mutation H168R rescues the function of R249S in a specific manner by mimicking the structural role of Arg-249 in the wild type (16).

Author contributions: A.C.J. and A.R.F. designed research; A.C.J. and H.C.A. performed research; A.C.J. and H.C.A. analyzed data; and A.C.J. and A.R.F. wrote the paper.

The authors declare no conflict of interest.

Abbreviation: PDB, Protein Data Bank.

Data deposition: The atomic coordinates and structure factors have been deposited in the Protein Data Bank, www.pdb.org (PDB ID codes 2J1W, 2J1X, 2J1Y, 2J1Z, 2J20, and 2J21).

*To whom correspondence should be addressed. E-mail: arf25@cam.ac.uk.

Here, we extend our crystallographic studies on the p53 core domain to obtain a more comprehensive picture of the effects of common cancer mutations on the structure and function of p53. Using a stabilized variant of the p53 core domain (*T*-p53C), we have elucidated the diverse structural effects of cancer hotspot mutations in the DNA-binding surface (G245S, R273C, and R282W) and at the periphery of the β-sandwich (Y220C), as well as the effects of highly destabilizing, cavity-creating mutations (V143A and F270L) in the hydrophobic core of the β-sandwich region of the protein (Fig. 1).

Results and Discussion

We focused our crystallographic studies on cancer-hotspot mutations in the DNA-binding surface (G245S, R273C, and R282W) and at the far end of the β-sandwich (Y220C), as well as on two potentially cavity-creating cancer mutations (V143A and F270L) in the hydrophobic core of the β-sandwich (Fig. 1). To do this, we introduced these mutations into a stabilized variant of p53 core domain (*T*-p53C). *T*-p53C contains four point mutations (M133L, V203A, N239Y, and N268D) that stabilize the core domain by 2.6 kcal/mol. It has wild-type-like DNA-binding properties, its full-length version is fully active in human cells (Sebastian Mayer and A.R.F., unpublished data), and the structure is essentially the same as that of the wild type, apart from the mutated side chains, which confer additional stability (17). The effects of the mutations are simply to raise the T_m of the protein and its mutants by 6°C, making them easier to handle (18).

The crystallization conditions for five of the six mutants were similar to those for *T*-p53C, and the obtained crystals were isomorphous. They belonged to space group $P2_12_12_1$ with two molecules in the asymmetric unit, and the corresponding structures were determined at high resolution ranging from 1.6 to 1.8 Å (Table 1, which is published as supporting information on the PNAS web site). In all of these five constructs containing an extended C terminus (residues 94–312), the C-terminal residues beyond Lys-291 were disordered, as found previously (5, 16, 17). For *T*-p53C-G245S, a shorter construct was used (residues 94–293), and we obtained crystals in a new crystal form (space group $P2_1$ with four molecules in the asymmetric unit), which allowed us to determine the structure at 1.69-Å resolution (Table 1). The structural studies were complemented by urea denaturation studies to determine the effects of mutation on the thermodynamic stability of the protein (Table 2, which is published as supporting information on the PNAS web site).

R273C and R273H Are Classic Contact Mutants. R273C and R273H are two of the five most frequent cancer-associated mutations. They affect Arg-273, which makes major contacts with the phosphate backbone of target DNA. Having previously solved the crystal structure of *T*-p53C-R273H (16), we have now determined the structure of *T*-p53C-R273C (at 1.8-Å resolution) to elucidate the structural changes in the cysteine variant. Overall, the structures of *T*-p53C, *T*-p53C-R273H, and *T*-p53C-R273C are virtually identical. A pairwise superposition of the C^α atoms from equivalent chains gives rmsds of <0.16 Å. The R273C mutation simply removed a DNA contact without perturbing the conformation of neighboring residues, such as Phe-134 and Asp-281 (Fig. 2). The preservation of the overall architecture of the DNA-binding surface in the structures of *T*-p53C-R273C and *T*-p53C-R273H explains why these mutants exhibit residual DNA-binding activity despite the loss of a crucial DNA contact (ref. 18 and unpublished data).

G245S Induces Small Conformational Changes in the L3 Loop. The G245S mutation is located in the L3 loop, which binds to the minor groove of DNA response elements via Arg-248 (Fig. 1). The crystal structure of *T*-p53C-G245S revealed distinct structural changes in the immediate environment of the mutation site. Observed conformational changes in some surface loops (e.g., in the L1 loop and the S7–S8 loop) can be attributed to differences in crystallization conditions and crystal packing for *T*-p53C and *T*-p53C-G245S and reflect the intrinsic conformational flexibility of these loop regions (12, 17, 19). In *T*-p53C-G245S, the hydroxyl group of Ser-245 points toward the zinc ligands Cys-238 and Cys-242 and displaces a structural water molecule that is observed in the wild-type and various mutant structures (Fig. 3*A*). The main-chain atoms of Ser-245 form the same hydrogen bonds with neighboring residues (Cys-242 and the side chain of Arg-249) as observed for the glycine in the wild type and *T*-p53C, although the backbone conformation of Ser-245 is slightly different. Both dihedral angles ϕ and ψ have changed by ≈20° and fall within a "generously allowed" region of the Ramachandran plot ($\phi = -141°$, $\psi = -102°$). As such, Ser-245 adopts a moderately unfavorable main-chain conformation.

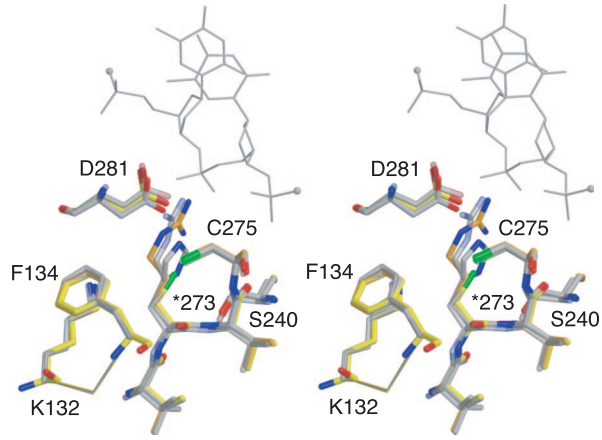

Fig. 2. Crystal structure of *T*-p53C-R273C. Stereoview of the mutation site in the structure of *T*-p53C-R273C [Protein Data Bank (PDB) ID code 2J20, yellow] superimposed on the structure of *T*-p53C (PDB ID code 1UOL, orange), *T*-p53C-R273H (PDB ID code 2BIM, gray), and DNA-bound wild type (PDB ID code 1TSR, light gray). One strand of bound DNA in the vicinity of Arg-273 is shown as a gray line, with small spheres indicating the continuation of the DNA backbone.

Most interestingly, the mutation appears to trigger a flip of the peptide bond between Met-243 and Gly-244, resulting in a displacement of the corresponding C^α atoms by 0.7 and 1.7 Å, respectively. This peptide flip relative to the conformation found in the structures of *T*-p53C and DNA-bound wild type was observed in all four molecules of the asymmetric unit. There is also a significant structural response from Pro-177, which follows the movement of Gly-244 to avoid steric clashes and is shifted to a similar extent. The backbone conformation of residues 246–250 of the L3 loop, which includes the DNA-contact residue Arg-248, is only marginally affected, and their C^α displacements are in the 0.5-Å range. Some of the residues with the most significant shifts in their C^α atoms (Met-243, Gly-244, and Pro-177), however, are key residues in the subunit interface of the core domain dimer bound to a DNA half-site (10, 20, 21). (Fig. 3*C*). Although the G245S mutation has no major direct effect on the DNA-contact residue Arg-248 in the DNA-free form of *T*-p53C-G245S, it presumably puts conformational strain on the subunit interface upon DNA binding. Such effects on the subunit interface would explain DNA-binding studies on full-length *T*-p53-G245S, which show that specific binding to the *gadd45* response element is ≈15-fold reduced relative to *T*-p53 at physiological ionic strength (18). In contrast, R249S, the other structural cancer hotspot mutation in the L3 loop, substantially

BIOPHYSICS

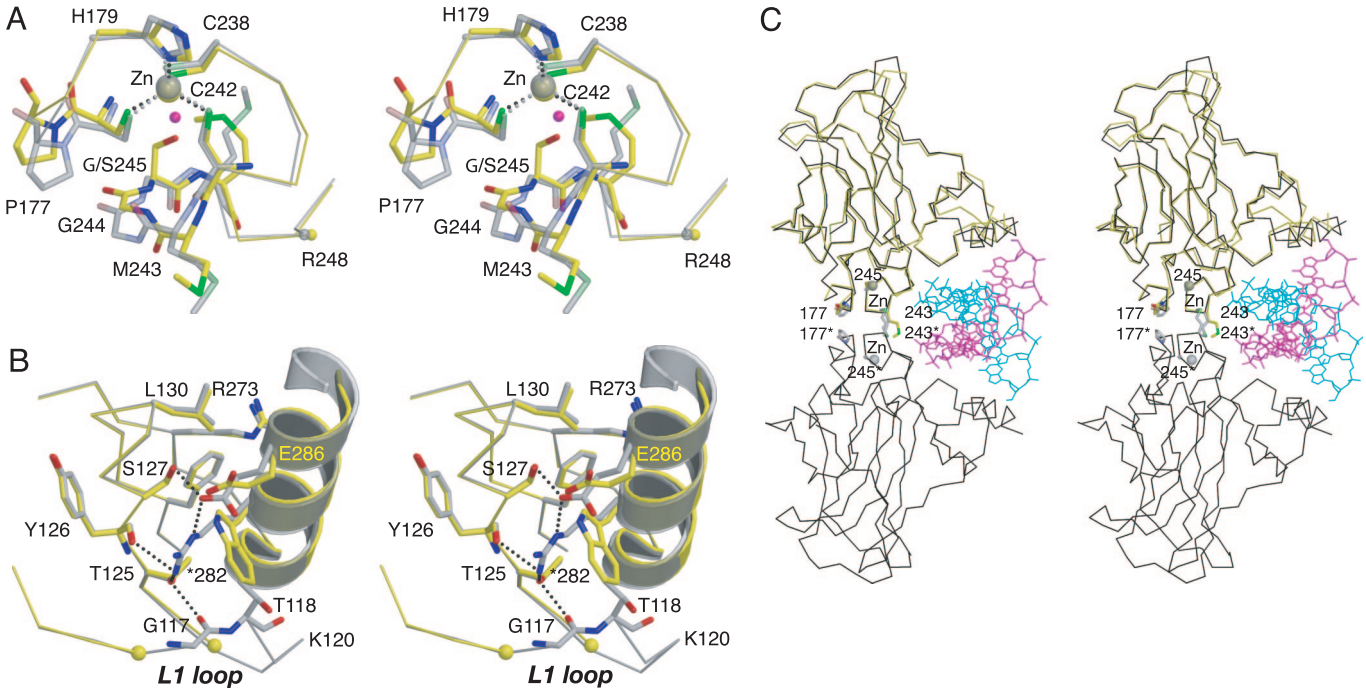

Fig. 3. Structural effects of the cancer mutations G245S and R282W. (*A*) Stereoview of the zinc-binding region of *T*-p53C-G245S (PDB ID code 2J1Y, molecule A, yellow) superimposed on the structure of *T*-p53C (PDB ID code 1UOL, molecule A, gray). The C^{α} atom of the DNA-contact residue Arg-248 is depicted as a small sphere in the color of the corresponding chain. A structural water molecule that is present in *T*-p53C but displaced by the side chain of Ser-245 in *T*-p53C-G245S is shown as a magenta sphere. (*B*) Stereoview of the loop–sheet–helix motif in the crystal structure of *T*-p53C-R282W (PDB ID code 2J21, molecule A, yellow) superimposed on *T*-p53C (PDB ID code 1UOL, molecule A, gray). Stabilizing interactions mediated via Arg-282 in *T*-p53C are shown as dotted lines. Residues 117–121 of *T*-p53C-R282W were disordered. The C^{α} atoms on both sides of the chain break are highlighted by small yellow spheres. (*C*) C^{α} trace of a wild-type core domain dimer bound to a DNA half-site (PDB ID code 2AC0, black) (10). The two strands of bound DNA are shown in blue and magenta. *T*-p53C-G245S, shown in yellow, is superimposed on one of the two monomers. Selected residues at the core–core domain interface are highlighted.

perturbs the L3 loop, induces high flexibility, and favors alternative conformations with much more severe consequences for the overall protein stability and DNA binding (16, 18). Hence, for these two structural hotspot mutations in the L3 loop, there is a direct correlation between the magnitude of loss of DNA binding and the extent of the observed structural perturbation.

Our structures also explain interactions of p53 mutants with other proteins, such as the apoptosis-stimulating protein ASPP2. Under conditions where the mutants are fully folded, several cancer mutants bind to the 53BP2 domain of the ASPP2 protein at wild-type levels, whereas no binding is detected for the mutants *T*-p53C-R249S and *T*-p53C-G245S, which have distinct structural changes in the region that forms the central part of the p53–53BP2 interface (22).

The R282W Mutation Affects the Packing of the Loop–Sheet–Helix Motif. Arg-282 plays a crucial role in maintaining the structural integrity of the loop–sheet–helix motif that binds to the major groove of DNA target sites (Fig. 1). Its side chain is involved in a network of interactions that pack helix H2 against the S2–S2′ β-hairpin and loop L1 (Fig. 3*B*). The 1.6-Å crystal structure of *T*-p53C-R282W revealed that the overall fold of the protein is not compromised by the R282W hotspot mutation. The C^{α} atoms of *T*-p53C-R282W and *T*-p53C can be superimposed with a rmsd of 0.26 Å. There are, however, substantial structural perturbations in the loop–sheet–helix motif (Fig. 3*B*), and several stabilizing interactions are lost, which accounts for the loss of thermodynamic stability of 3 kcal/mol. The region of the L1 loop next to Trp-282 is disordered because of steric hindrance, and no conclusive electron density was observed for several residues within this loop (residues 117–121, including the DNA contact Lys-120). As such, Trp-282 displaces what appears to be the weakest structural link in the loop–sheet–helix motif. The side chain of Trp-282 is solvent-exposed and much less well embedded within the protein structure than the arginine in *T*-p53C. The destabilization of the loop–sheet–helix motif is also reflected in the *B* factor profile, which shows an increased mobility for the main-chain atoms at both ends of the chain break in loop L1 and around the mutation site in the C-terminal helix, and this trend is propagated toward the chain end (Fig. 6, which is published as supporting information on the PNAS web site). The overall packing characteristics of the C-terminal helix containing the DNA-contact residues Cys-277 and Arg-280 against the core of the protein, however, are preserved. Hence, at the subphysiological temperatures at which the mutant R282W is largely folded, it is still able to bind *gadd45* DNA (14) despite the structural disorder in the L1 loop containing the DNA-contact residue Lys-120. This retention of binding activity is consistent with a recent mutational analysis of the L1 loop (23) and with the observation that this loop is a mutational "cold spot" that is only rarely mutated in human cancer (3), indicating that structural perturbations in the L1 loop are tolerated to a certain degree without abrogating p53 function.

Y220C Creates a Solvent-Accessible Cleft at the Periphery of the β-Sandwich. Y220C is the most common cancer mutation outside the DNA-binding surface (compare release R10 of the TP53 mutation database at www-p53.iarc.fr) (3). It is located at the far end of the β-sandwich, at the start of the loop connecting β-strands S7 and S8 (Fig. 1) and destabilizes the core domain by 4 kcal/mol (Table 2). The benzene moiety of Tyr-220 forms part of the hydrophobic core of the β-sandwich, whereas the hydroxyl group points toward the solvent. The 1.65-Å crystal structure of

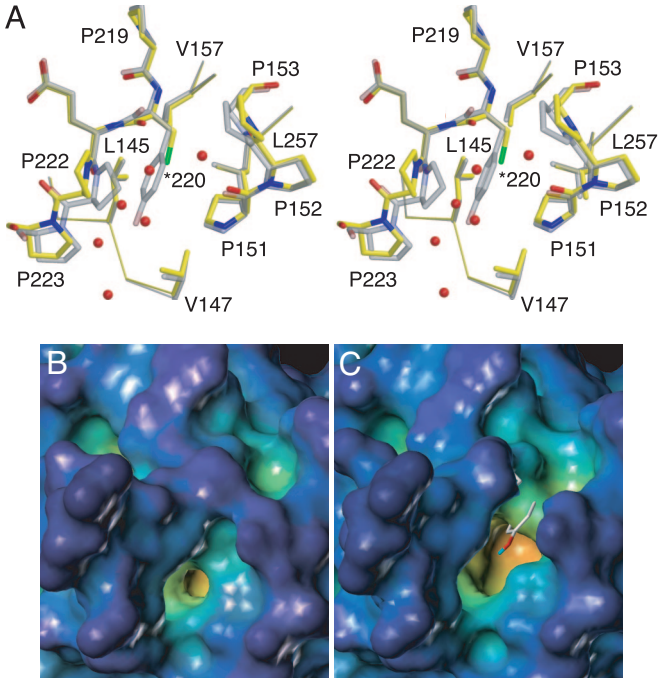

Fig. 4. Crystal structure of *T*-p53C-Y220C. (*A*) Stereoview of the mutation site at the periphery of the β-sandwich in *T*-p53C-Y220C (PDB ID code 2J1X, molecule A, yellow) superimposed on the structure of *T*-p53C (PDB ID code 1UOL, molecule A, gray). Several water molecules close to Cys-220 in *T*-p53C-Y220C that fill the cleft created by the mutation are shown as red spheres. (*B*) Molecular surface of *T*-p53C around Tyr-220. (*C*) Molecular surface of *T*-p53C-Y220C. The view is the same as in *B*. The position of the side chain of Tyr-220 in *T*-p53C is shown as a stick model.

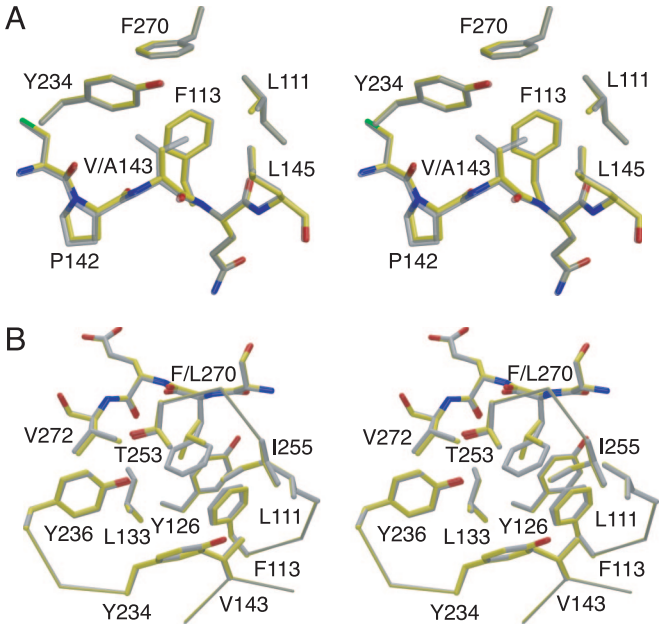

Fig. 5. Crystal structures of *T*-p53C-V143A and *T*-p53C-F270L. (*A*) Stereoview of the structure of *T*-p53C-V143A (PDB ID code 2J1W, yellow) superimposed on *T*-p53C (PDB ID code 1UOL, gray). All residues in the hydrophobic core of the β-sandwich within a 4.5-Å radius of the Val-143 side chain in *T*-p53C are shown. (*B*) Stereoview of the structure of *T*-p53C-F270L (PDB ID code 2J1Z, yellow) superimposed on *T*-p53C (PDB ID code 1UOL, gray). All residues within a 6-Å radius of the Phe-270 side chain in *T*-p53C are shown.

T-p53C-Y220C showed that the Y220C mutation creates a solvent-accessible cleft that is filled with water molecules at defined positions but leaves the overall structure of the core domain intact (Fig. 4). The structural changes upon mutation link two rather shallow surface clefts, preexisting in the wild type, to form a long, extended crevice in *T*-p53C-Y220C, which has its deepest point at the mutation site (Fig. 4 *B* and *C*). Cys-220 occupies approximately the position of the equivalent atoms of Tyr-220 in the wild type. The positions of neighboring hydrophobic side chains located in the core of the β-sandwich have not shifted significantly. The mutation, however, results in a loss of hydrophobic interactions and a suboptimal packing of these hydrophobic core residues. The side chain of Leu-145, which was buried in the wild type, for instance, becomes partly solvent accessible in *T*-p53C-Y220C. The largest structural changes in the immediate environment of the mutation site are found in the S7–S8 loop for Pro-222. Throughout the structure, there is no C^{α} displacement >0.9 Å.

β-Sandwich Mutations and the Molecular Basis of Temperature Sensitivity. About one-third of the reported cancer mutations in the p53 core domain are located outside the structural elements that form the DNA-binding surface (loops L2 and L3 and the loop–sheet–helix motif). The V143A mutant is of particular interest because of the well documented temperature sensitivity of its binding to many response elements in both yeast and mammalian systems. At body temperature, the mutant is inactive and unfolded, whereas it retains transactivational activity at lower temperatures (24, 25). The structures of *T*-p53C-V143A and *T*-p53C-F270L provide the molecular basis for understanding the temperature-sensitive behavior of many β-sandwich mutants. Both mutations created internal cavities in the hydrophobic core of the β-sandwich without collapse of the surrounding structure (Fig. 5). The cavity volume was 47 $Å^3$ (*T*-p53C-V143A) and 51 $Å^3$ (*T*-p53C-F270L), as defined by the volume that can be occupied by a probe mimicking the size of a water molecule (1.4-Å probe radius). Additional information on these cavities is provided in Table 3, which is published as supporting information on the PNAS web site. In agreement with the hydrophobic nature of the cavities, no ordered buried water molecules were detected in the crystal structure. Although the overall structure of the core domain was perfectly conserved, the creation of void volumes came at a high energetic cost of 3.7 and 4.1 kcal/mol. These observations are consistent with studies on "large-to-small" substitutions in the hydrophobic core of T4-lysozyme and barnase (26–28).

A recent study has identified a large number of temperature-sensitive p53 mutants (29). Most mutations were clustered in the β-sheet region of the protein, and the substitutions were mainly from large hydrophobic residues to smaller hydrophobic residues. Incidentally, V143A was not detected in this study, whereas mutations at residue 270 were (F270I and F270C). Interestingly, the Y220C mutation has also been reported to cause temperature-sensitive behavior (25). Again, this behavior is in agreement with our crystallographic data, which show that the mutation-induced structural changes are very localized, far away from the DNA-binding surface. A common structural feature of the β-sandwich mutants seemed to be that there were only minor structural disruptions upon mutation, although the effect on the thermodynamic stability of the protein was generally more severe than for the hotspot mutations in the DNA-binding surface. The much more compact and robust structural framework of the β-sandwich compared with the zinc-binding region and the loop–sheet–helix motif renders it generally much less susceptible to mutation-induced structural changes, in particular for large-to-small substitutions. The absence of structural

changes in surface regions, especially in the DNA-binding surface, however, is key for functionality. Hence, temperature-sensitive behavior can be expected for all cancer mutations that destabilize the core domain without compromising the surface complementarity that is crucial to the function of p53, not only for binding to specific promoter sequences but also for interactions with regulatory proteins and for correct domain organization in tetrameric full-length p53 (9, 30–33).

Implications for Rescue Strategies. At first glance, the discussion of the local structural changes induced by highly destabilizing mutations appears to be rather academic when assessing the functional consequences under physiological conditions, because these mutant proteins will most likely be largely unfolded. Our structural observations, however, have profound implications for therapeutic strategies that aim to rescue the function of p53 with small-molecule drugs that stabilize p53 (reviewed in refs. 34 and 35). The mutations N239Y and N268D have been reported to restore transcriptional activity in a subset of cancer mutants, including G245S (36). Double-mutant cycles suggest that they act as global stability suppressors (37). As such, they mimic the effects of a hypothetical generic small-molecule drug. The structure of *T*-p53C-G245S, however, exhibits distinct structural perturbations despite the presence of these stabilizing suppressor mutations, concomitant with altered functional properties (e.g., impaired binding of 53BP2; see above). For mutants with local structural changes in the DNA-binding surface, simple stabilization by means of a generic small molecule may not be enough to fully restore activity. A prime example is the mutant R249S. Studies on second-site suppressor mutations have shown that full restoration of DNA-binding activity is found only in the presence of a mutation (H168R) that specifically reverses the structural changes induced by the oncogenic mutation (16, 36, 37).

On the basis of our structural studies, β-sandwich mutants, such as V143A and F270L, represent much more promising targets for rescue by generic small-molecule drugs, because, in this case, stabilizing the wild-type conformation of the protein by ligand binding may be sufficient to restore wild-type-like activity under physiological conditions. The Y220C mutant not only has the potential of being rescued by a generic wild-type-binding compound but also has the possibility of being a target for a mutant-selective drug that can bind in the crevice formed by the deletion (Fig. 4*C*). This crevice region is particularly attractive because it appears to be distant from the functional sites and interfaces of the protein.

What Makes Human Alleles Deleterious? It is estimated that ≈20% of common nonsynonymous single-nucleotide polymorphisms result in amino acid changes that damage the corresponding protein, resulting in ≈2,000 potentially deleterious alleles in the average human genotype (38). The structural and energetic response of the p53 core domain to the V143A and F270L mutations in the hydrophobic core of the β-sandwich suggests that this type of mutation results in deleterious phenotypes mainly because p53 is only marginally stable at body temperature. Equivalent mutations in a more stable structural scaffold may have only subtle effects on function and result in rather neutral phenotypes.

There is growing evidence that p53 has evolved to be highly dynamic and intrinsically unstable (12, 19, 39). As a negative side effect of this evolutionary process, the core domain of p53 has in a way become more susceptible to cancer-associated mutations in the β-sandwich. To our knowledge, there has been no comprehensive quantitative study on the stability of human proteins. It would be interesting to address the question of whether the low intrinsic thermodynamic stability of p53 is the exception or a common feature of highly regulated multifunctional proteins at pivotal cellular checkpoints, as also observed in the case of the tumor suppressor protein p16, for example (40). Such knowledge combined with more structural data on the effect of mutations would significantly improve predictions as to whether nonsynonymous single-nucleotide polymorphisms are benign or likely to cause functional disorders.

Conclusion

Our crystallographic studies paint an intriguing picture of the effects of p53 cancer mutations. They clearly show that the mutations result in a variety of characteristic structural changes, concomitant with distinct energetic responses, although the overall structural framework is largely conserved. Accordingly, general conclusions about "mutant p53" based on the results obtained for one particular mutant have to be treated with caution. Two aspects have to be considered when rationalizing functional properties of a particular cancer mutant, even though there is a direct causal connection between the two: (*i*) the effect of mutation on the overall thermodynamic stability of the protein and (*ii*) the nature of local conformational changes. The effects on thermodynamic stability will determine whether a mutant is folded at a particular temperature. Whether a mutant is functional in the folded state, however, depends on the extent and nature of the structural changes, in particular in the DNA-binding surface, which will eventually determine the selectivity for various response elements or the interactions with other proteins, such as apoptotic cofactors. Recent studies in yeast and mammalian cell lines have shown that different mutants exhibit distinct transactivation patterns that are directly connected with different phenotypes (41, 42). More importantly, a study involving breast cancer patients suggested that different p53 mutations are associated with different prognostic values (43). These observations highlight the need for a thorough understanding of the mutation–structure and structure–function relationship in p53 so that biological outcome and response to drug treatment can be predicted. The details of individual structures point toward the possibility of designing specific drugs to bind to them and stabilize the native conformation.

Materials and Methods

Mutagenesis and Protein Purification. Mutagenesis, gene expression, and protein purification were performed as described in ref. 16, with a modification for *T*-p53C-G245S, for which a shortened construct comprising residues 94–293 (instead of 94–312) was used. After the final purification step (gel filtration), the mutant proteins were concentrated to 6–7 mg/ml, flash-frozen, and stored in liquid nitrogen.

Equilibrium Denaturation. Urea denaturation studies were performed as described in ref. 16 by using the equations described in ref. 14 for data analysis.

Crystallization and Structure Determination. All crystals were grown at 17°C by using the sitting drop vapor-diffusion technique. Crystals of *T*-p53C-V143A, *T*-p53C-Y220C, *T*-p53C-F270L, and *T*-p53C-R282W were grown under the conditions described for *T*-p53C (17); crystals of *T*-p53C-R273C were grown under the conditions described for *T*-p53C-R273H (16). Crystals of *T*-p53C-G245S were grown by mixing 2 μl of protein solution (6 mg/ml) with 0.4 μl of water and 1.6 μl of the reservoir solution (19% polyethylene glycol 3350/0.19 M calcium acetate, pH 7.2). Crystals were flash-frozen in liquid nitrogen by using mother liquor with either 20% polyethylene glycol 200 or 20% glycerol as a cryoprotectant. X-ray data sets were collected at 100 K on beamlines 10.1 and 14.1 at the Synchrotron Radiation Source (Daresbury, U.K.). Data processing was performed by using Mosflm (44) and Scala (45). All crystals except *T*-p53C-G245S belonged to space group $P2_12_12_1$ with two molecules per asym-

metric unit and were isomorphous to those obtained for *T*-p53C and *T*-p53C-R273H (16, 17). Structure solution and refinement were performed with CNS (46). After an initial round of rigid-body refinement using the structure of either *T*-p53C (PDB ID code 1UOL) or *T*-p53C-R273H (PDB ID code 2BIM) as a starting model, the structures were refined by iterative cycles of refinement with CNS and manual model-building with MAIN (47). Crystals of *T*-p53C-G245S belonged to space group $P2_1$ with four molecules per asymmetric unit. The structure was solved by molecular replacement with CNS using *T*-p53C as a search model. Subsequent refinement was performed as described above for the other mutants. The final models (1.6- to 1.8-Å resolution) had a crystallographic *R* factor of 18.3–19.8% (R_{free} = 20.6–22.3%) and excellent stereochemistry as verified with PROCHECK (48). Detailed data collection and refinement statistics are summarized in Table 1.

Structure Analysis. Unless otherwise stated, detailed descriptions of mutant structures are based on the comparison of molecule A of a particular mutant with molecule A of *T*-p53C. Numbering of secondary structure elements is as reported for the wild-type structure in complex with DNA (5) [e.g., loop L2 comprises residues 164–194, including a short helix (H1)]. Depending on the program used to assign secondary structure, the β-turn region at the beginning of the L2 loop is sometimes alternatively assigned as a short 3_{10}-helix. Volumes of internal cavities were calculated with VOIDOO (49) by using different probe sizes (1.4- and 1.2-Å radius). Calculations were performed for 10 random orientations of the molecule. The cavity refinement parameters were as described in ref. 28. Structural figures were prepared by using MOLSCRIPT (50), RASTER3D (51), and SYBYL 6.9 (Tripos, St. Louis, MO).

We thank Caroline Blair for protein purification, Fiona Sait for setting up crystallization trials for *T*-p53C-G245S, Dr. Frank Boeckler for help generating Fig. 4 *B* and *C*; and the staff at the Synchrotron Radiation Source for helpful advice and assistance in data collection. This work was supported by the Agency for Science, Technology, and Research of Singapore (H.C.A.), Cancer Research UK, the Medical Research Council, and European Community FP6 funding.

1. Vogelstein B, Lane D, Levine AJ (2000) *Nature* 408:307–310.
2. Vousden KH, Lu X (2002) *Nat Rev Cancer* 2:594–604.
3. Olivier M, Eeles R, Hollstein M, Khan MA, Harris CC, Hainaut P (2002) *Hum Mutat* 19:607–614.
4. Beroud C, Soussi T (2003) *Hum Mutat* 21:176–181.
5. Cho Y, Gorina S, Jeffrey PD, Pavletich NP (1994) *Science* 265:346–355.
6. Clore GM, Ernst J, Clubb R, Omichinski JG, Kennedy WM, Sakaguchi K, Appella E, Gronenborn AM (1995) *Nat Struct Biol* 2:321–333.
7. Jeffrey PD, Gorina S, Pavletich NP (1995) *Science* 267:1498–1502.
8. Bell S, Klein C, Muller L, Hansen S, Buchner J (2002) *J Mol Biol* 322:917–927.
9. Veprintsev DB, Freund SM, Andreeva A, Rutledge SE, Tidow H, Canadillas JM, Blair CM, Fersht AR (2006) *Proc Natl Acad Sci USA* 103:2115–2119.
10. Kitayner M, Rozenberg H, Kessler N, Rabinovich D, Shaulov L, Haran TE, Shakked Z (2006) *Mol Cell* 22:741–753.
11. Ho WC, Fitzgerald MX, Marmorstein R (2006) *J Biol Chem* 281:20494–20502.
12. Canadillas JM, Tidow H, Freund SM, Rutherford TJ, Ang HC, Fersht AR (2006) *Proc Natl Acad Sci USA* 103:2109–2114.
13. Bullock AN, Fersht AR (2001) *Nat Rev Cancer* 1:68–76.
14. Bullock AN, Henckel J, Fersht AR (2000) *Oncogene* 19:1245–1256.
15. Wong KB, DeDecker BS, Freund SM, Proctor MR, Bycroft M, Fersht AR (1999) *Proc Natl Acad Sci USA* 96:8438–8442.
16. Joerger AC, Ang HC, Veprintsev DB, Blair CM, Fersht AR (2005) *J Biol Chem* 280:16030–16037.
17. Joerger AC, Allen MD, Fersht AR (2004) *J Biol Chem* 279:1291–1296.
18. Ang HC, Joerger AC, Mayer S, Fersht AR (2006) *J Biol Chem* 281:21934–21941.
19. Pan Y, Ma B, Levine AJ, Nussinov R (2006) *Biochemistry* 45:3925–3933.
20. Rippin TM, Freund SM, Veprintsev DB, Fersht AR (2002) *J Mol Biol* 319:351–358.
21. Klein C, Planker E, Diercks T, Kessler H, Kunkele KP, Lang K, Hansen S, Schwaiger M (2001) *J Biol Chem* 276:49020–49027.
22. Tidow H, Veprintsev DB, Freund SM, Fersht AR (2006) *J Biol Chem*, 10.1074/jbc.M604725200.
23. Zupnick AE, Prives C (2006) *J Biol Chem* 281:20464–20473.
24. Zhang W, Guo XY, Hu GY, Liu WB, Shay JW, Deisseroth AB (1994) *EMBO J* 13:2535–2544.
25. Di Como CJ, Prives C (1998) *Oncogene* 16:2527–2539.
26. Xu J, Baase WA, Baldwin E, Matthews BW (1998) *Protein Sci* 7:158–177.
27. Buckle AM, Henrick K, Fersht AR (1993) *J Mol Biol* 234:847–860.
28. Buckle AM, Cramer P, Fersht AR (1996) *Biochemistry* 35:4298–4305.
29. Shiraishi K, Kato S, Han SY, Liu W, Otsuka K, Sakayori M, Ishida T, Takeda M, Kanamaru R, Ohuchi N, *et al.* (2004) *J Biol Chem* 279:348–355.
30. Derbyshire DJ, Basu BP, Serpell LC, Joo WS, Date T, Iwabuchi K, Doherty AJ (2002) *EMBO J* 21:3863–3872.
31. Joo WS, Jeffrey PD, Cantor SB, Finnin MS, Livingston DM, Pavletich NP (2002) *Genes Dev* 16:583–593.
32. Gorina S, Pavletich NP (1996) *Science* 274:1001–1005.
33. Friedler A, Veprintsev DB, Rutherford T, von Glos KI, Fersht AR (2005) *J Biol Chem* 280:8051–8059.
34. Bykov VJ, Selivanova G, Wiman KG (2003) *Eur J Cancer* 39:1828–1834.
35. Wiman KG (2006) *Cell Death Differ* 13:921–926.
36. Brachmann RK, Yu K, Eby Y, Pavletich NP, Boeke JD (1998) *EMBO J* 17:1847–1859.
37. Nikolova PV, Wong KB, DeDecker B, Henckel J, Fersht AR (2000) *EMBO J* 19:370–378.
38. Sunyaev S, Ramensky V, Koch I, Lathe W, III, Kondrashov AS, Bork P (2001) *Hum Mol Genet* 10:591–597.
39. Huyen Y, Jeffrey PD, Derry WB, Rothman JH, Pavletich NP, Stavridi ES, Halazonetis TD (2004) *Structure (London)* 12:1237–1243.
40. Tang KS, Guralnick BJ, Wang WK, Fersht AR, Itzhaki LS (1999) *J Mol Biol* 285:1869–1886.
41. Resnick MA, Inga A (2003) *Proc Natl Acad Sci USA* 100:9934–9939.
42. Menendez D, Inga A, Resnick MA (2006) *Mol Cell Biol* 26:2297–2308.
43. Olivier M, Langerod A, Carrieri P, Bergh J, Klaar S, Eyfjord J, Theillet C, Rodriguez C, Lidereau R, Bieche I, *et al.* (2006) *Clin Cancer Res* 12:1157–1167.
44. Leslie AGW (1992) *Joint CCP4 and ESF-EACMB Newsletter on Protein Crystallography* (Daresbury Lab, Warrington, UK), Vol 26.
45. Collaborative Computational Project, Number 4 (1994) *Acta Crystallogr D* 50:760–763.
46. Brünger AT, Adams PD, Clore GM, DeLano WL, Gros P, Grosse-Kunstleve RW, Jiang J-S, Kuszewski J, Nilges M, Pannu NS, *et al.* (1998) *Acta Crystallogr D* 54:905–921.
47. Turk D (1992) PhD thesis (Technische Universität, Munich).
48. Laskowski RA, MacArthur MW, Moss DS, Thornton JM (1993) *J Appl Crystallogr* 26:283–291.
49. Kleywegt GJ, Jones TA (1994) *Acta Crystallogr D* 50:178–185.
50. Kraulis PJ (1991) *J Appl Crystallogr* 24:946–950.
51. Merritt EA, Bacon DJ (1997) *Methods Enzymol* 277:505–524.